

Supplementary Information for:

Macroscopic Alignment of Block Copolymers on Silicon Substrates by Laser Annealing

Arkadiusz A. Leniart¹, Przemyslaw Pula¹, Andrzej Sitkiewicz¹, Pawel W. Majewski^{1*}

¹ Department of Chemistry, University of Warsaw, Warsaw, 02089, Poland

*Email: pmajewski@chem.uw.edu.pl

1. Optical setup

Figure S1 shows an overview of the optical system used in this study. The optical fiber output ($\varphi = 100 \mu\text{m}$, $NA = 0.22$, $P = 30 \text{ W}$) beam is collimated by a plano-convex lens ($F = +25 \text{ mm}$) and refocused by a plano-cylindrical lens ($F = +30 \text{ mm}$) into a $120 \mu\text{m}$ wide laser line. Both lenses are anti-reflection coated ($R_{980 \text{ nm}} < 0.5\%$) and the optical power losses ($\approx 10\%$) originate primarily from the reflections off the uncoated quartz vacuum window. The optical head is tilted in the plane of the sweep direction to avoid back-reflections of the beam into the optical system.

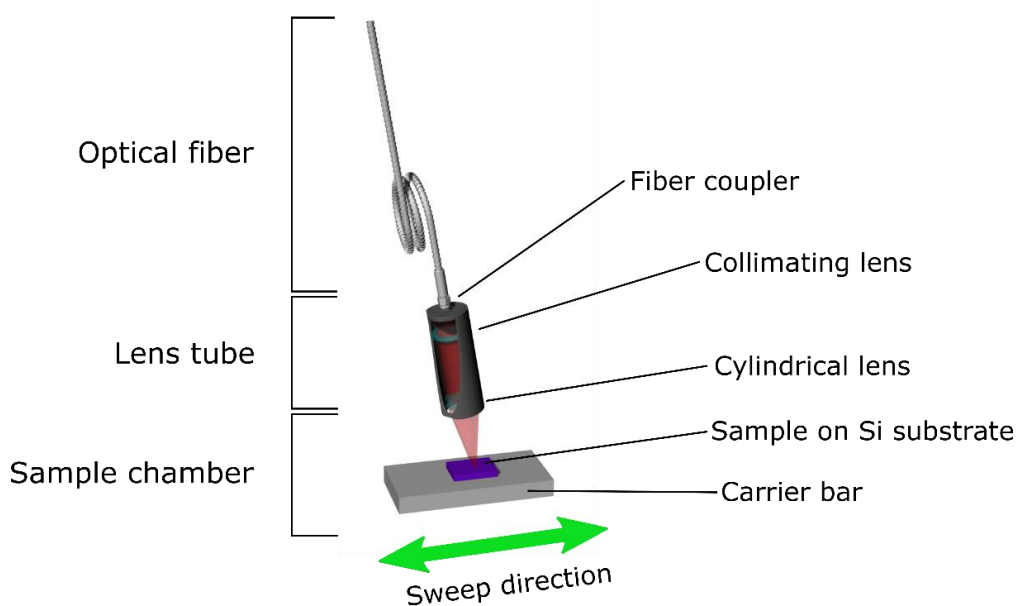


Figure S1. Overview of the optical setup. The vacuum chamber elements are not shown for clarity.

2. Laser power measurements

Laser power delivered to the sample was measured as a function of control voltage with a thermal power sensor (S370C, Thorlabs) after passage of all optical elements (*i.e.*, the laser head optics and the 5 mm thick quartz vacuum window). Since the maximum limit of CCW laser power measurement of the meter is 15 W (maximum 2 minutes exposure), we controlled laser duty-cycle by modulating the control signal with a 1 kHz square wave provided by a function generator (AFG-2005, GW Instek). A calibration curve (Figure S2) was obtained by extrapolating high-power (15–30 W) range data points to the 100% duty cycle.

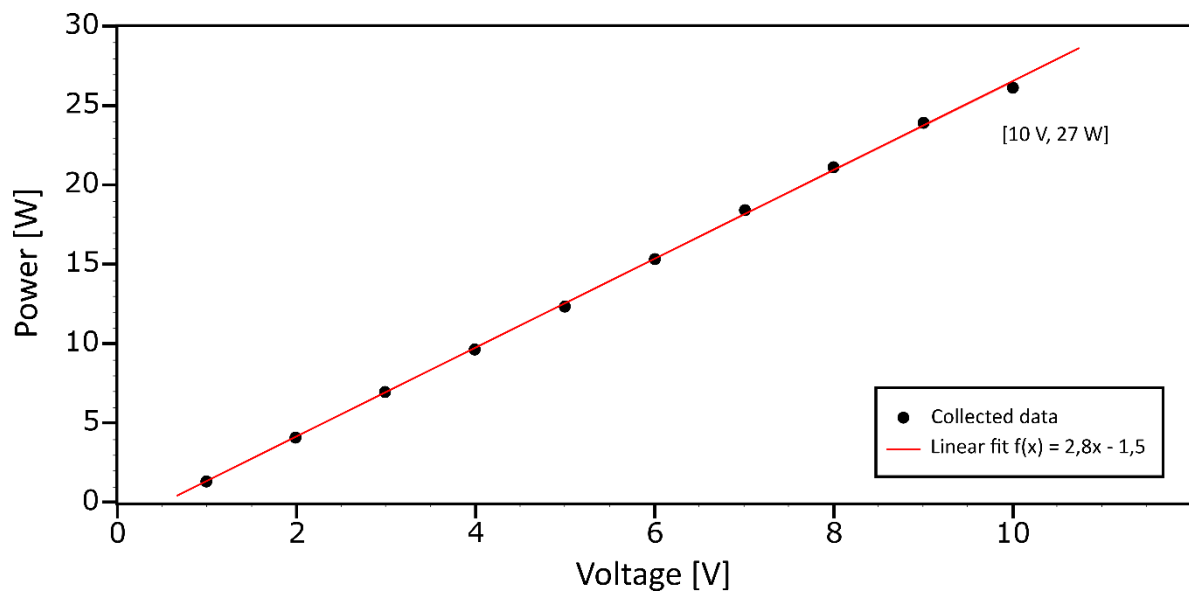


Figure S2. Laser power calibration. The red curve is a linear fit used as a reference for controlling laser power with analog voltage signal in laser annealing experiments.

3. Beam profiling

Focusing of the laser line at the plane of Si substrates was performed by micrometer-driven vertical translation of the optical head assembly and recording a series of beam images using a digital camera. The in-focus position was determined after analysis of cross-sectional profiles of the beam and finding the minimal width position.

Optical profile of the beam in focus shown in Figure S3a was recorded using a digital beam profiler (CinCam CMOS Nano, Cinogy). The optical profile along the laser line (Figure S3b) displays multiple maxima characteristic of a multimode beam. Despite the presence of several peaks and slight skewness of the profile due to the tilting of the optical head assembly, an envelope of the beam can be roughly approximated by a Gaussian function whose $fwhm_y = 4.65$ mm ($\sigma_y \approx 2.0$ mm).

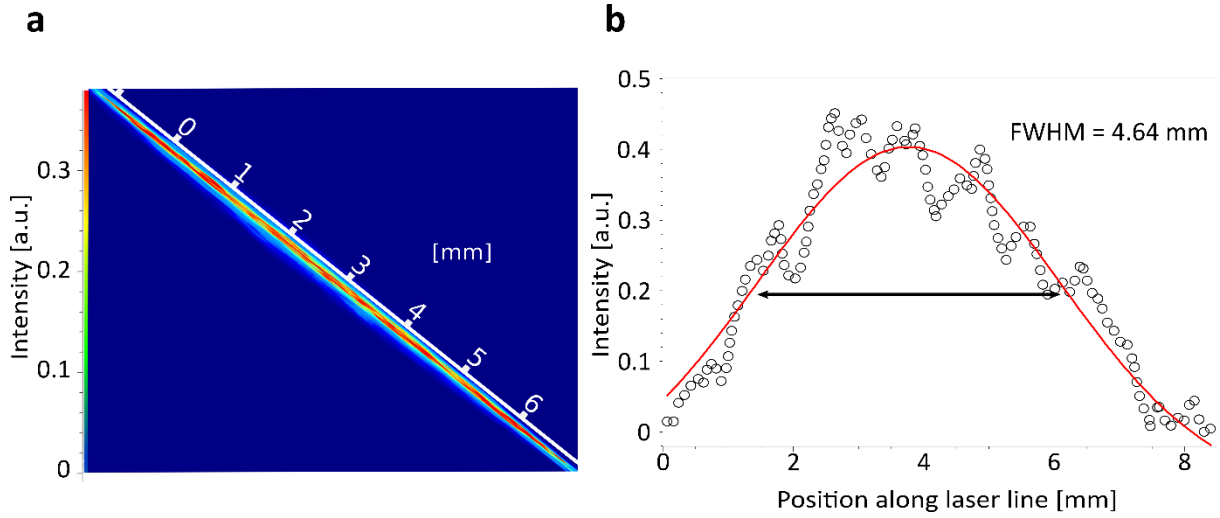


Figure S3. a) 2D laser line profile acquired at the in-focus position. b) Optical profile along the y -direction (long axis of the line) obtained after integrating the 2D profile with the experimental data shown as black open circles and a fit to a Gaussian function (red curve).

4. Surface thermometry

Surface temperature profiling was performed by utilizing a reference thermometric substance following a modified protocol of the previously described *melt-marks* analysis.¹ Silicon substrates were coated with a thin layer (≈ 100 nm) of tetrabutylammonium hexafluorophosphate (TBAHFP) deposited by spin-casting from acetone solution, followed by drying of residual solvent at 200 °C for 5 minutes. TBAHFP has a sharply-defined melting point at 245 °C and dewets silicon in the molten state. Under laser irradiation, thin layer of TBAHFP melts and dewets Si in a zone where $T \geq 245$ °C forming a characteristic melt-mark (Figure S4). The contour of the melt-mark is effectively constituting a 245 °C isotherm. A set of isotherms registered at various powers of illumination or base temperatures of the substrate can be used to reproduce the surface temperature profile extrapolated to particular power of optical illumination (*e.g.* the maximum optical power).

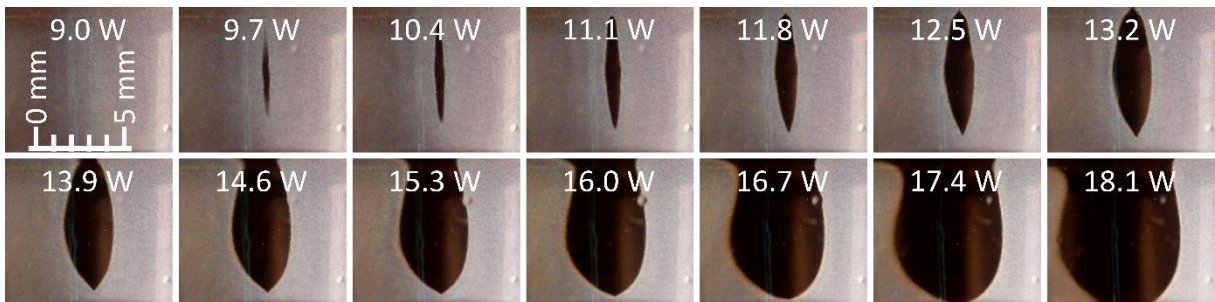


Figure S4. Melt-mark series at 100 °C base temperature recorded at increasing power of the laser.

A rise in temperature above the ambient (ΔT) at any given base temperature (T_{base}) can be rescaled to the value at the maximum power by using the following formula:

$$\Delta T_{max} = (245^{\circ}\text{C} - T_{base}) \cdot \frac{P_{max}}{P_{current}} \quad (1)$$

High power of illumination combined with low base temperature conditions are used to probe the central, hottest part of the profile. Conversely, utilizing higher base temperature allows registering the melt-marks at lower laser powers thus probing the low-temperature end of the maximum-power profile. The limit in the latter case is the maximum base temperature to which the system can be heated, typically defined by the thermal stability limits of gaskets and o-rings. To ensure reproducible results, the time of illumination of each melt-mark (30 s) was chosen to be long enough for the completion of TBAHFP dewetting process and is much longer than the characteristic heat-diffusion time required to reach a steady-state temperature profile in the sample (Figure S7b).

Although the low temperature points can be assessed by melt-mark analysis with a substance with lower melting temperature, we utilized a fine-gauge (0.1 mm) thermocouple attached to the surface of the wafer to measure temperature far away from the center of the laser line. Despite the simplicity of this approach, special care must be taken to affix the thermocouple junction to the wafer with a high-temperature cement to facilitate the flow of heat in vacuum. Also, direct illumination of the thermocouple wire or cement results in a steep increase in its temperature rendering which makes this method unsuitable for measuring temperatures near the laser line. The profile of Si surface temperature reconstructed using melt-mark analysis method and direct measurements with the thermocouple is shown in Figure S5.

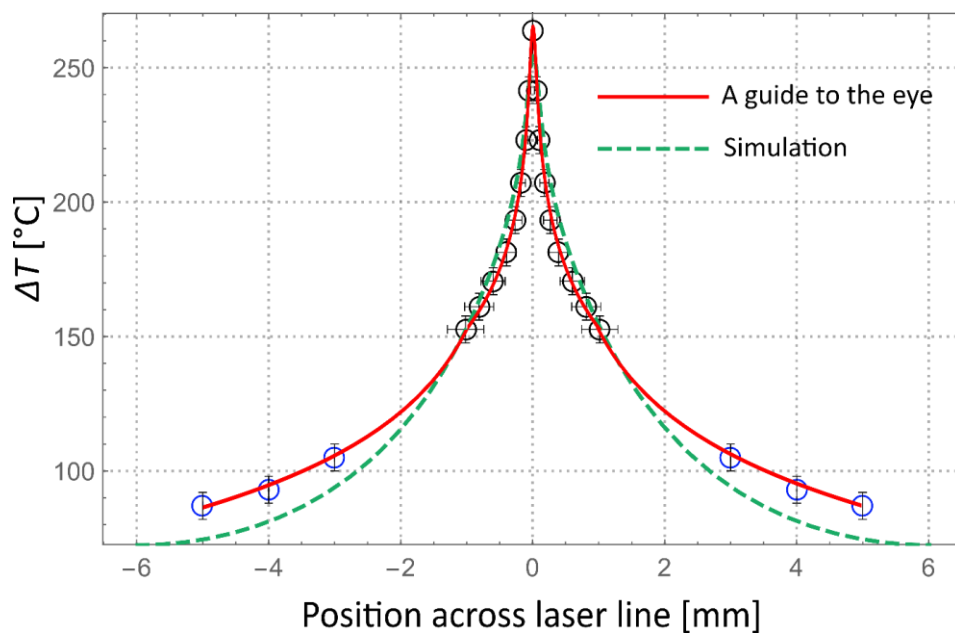


Figure S5. The rise in surface temperature of Si substrate after 30 s of illumination with 27 W, 980 nm highly-elongated Gaussian beam ($\sigma_x = 50 \mu\text{m}$ and $\sigma_y = 2.0 \text{ mm}$). Black circles represent temperature data points obtained through melt-mark analysis, blue circles – thermocouple measurements, the red curve is a guide to the eye. The green dashed curve represents the finite-element simulation results.

5. Numerical simulation of laser heating

Finite element simulation of laser heating was performed using COMSOL Multiphysics package. A model was built to evaluate thermal fields induced by laser illumination of the Si surface. An elongated 2D Gaussian profile ($\sigma_x = 50 \mu\text{m}$, $\sigma_y = 2.0 \text{ mm}$) was used to simulate the laser line. Due to a non-negligible depth of 980 nm photon absorption in silicon ($\approx 100 \mu\text{m}$ at 300 K)² compared to the thickness of the wafer (500 μm), the power deposited by the beam, Q was considered to be a volumetric source with the intensity per unit volume described by:

$$Q(x, y, z) = Q_o(1 - R) \frac{\alpha}{2\pi\sigma_x\sigma_y} e^{-x^2/2\sigma_x^2 - y^2/2\sigma_y^2} \cdot e^{-\alpha \cdot |z|} \quad (2)$$

Q_o is the optical power of the incident beam after the passage of all optical elements. The reflectance coefficient, R was assumed to be 31% (Figure S6, bare Si reflectance data) to match the conditions, under which the experimental thermometric data were obtained, *i.e.*, bare Si after the recession of the molten TBAHFP.

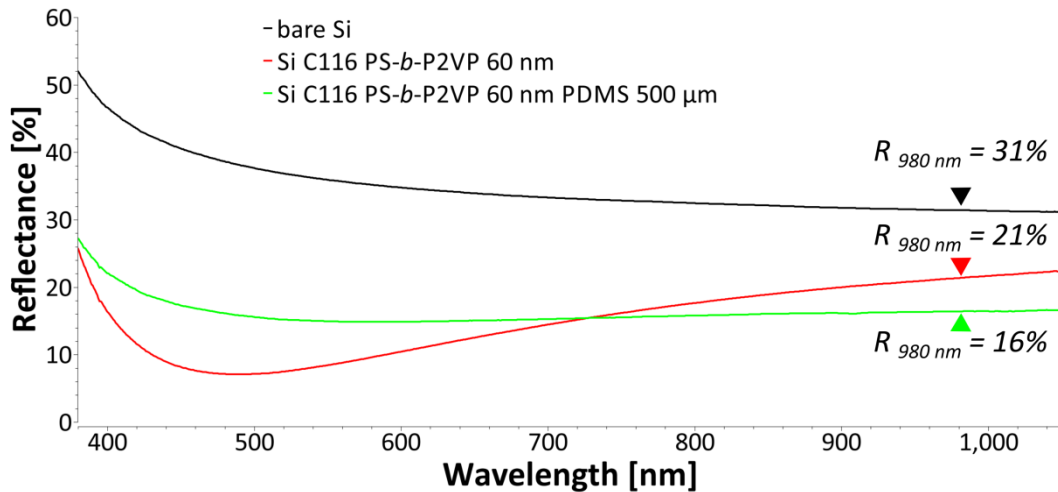


Figure S6. Spectral reflectance curves measured at normal incidence of light of bare Si (black), 60 nm PS-*b*-P2VP C116 on Si (red) and 60 nm PS-*b*-P2VP C116 on Si with a 500 μm pad of crosslinked PDMS elastomer (Sylgard 184).

The decrease in the absorption depth, strengthening the surface heating effects at elevated temperatures, was evaluated by extrapolating experimental room temperature absorption data (absorption coefficient $\alpha_{980 \text{ nm}} = 9.59 \times 10^2 \text{ m}^{-1}$, absorption depth $z_o = 102 \mu\text{m}$) reported by Green and Keevers² using empirical exponential temperature dependence found by Jellison and Modine.³

The simulated system shown in Figure S8a consisted of 12 mm \times 12 mm, 500 μm thick silicon chip resting on a carrier bar (15 mm \times 40 mm \times 4 mm) which in turn rested on a thick (100 mm \times 100 mm \times 10 mm) thermally-grounded base plate (isothermal boundary condition at the bottom surface). Both the carrier bar and the base plate were made of aluminum alloy (PA6, EN AW 2017). Thermal properties of the materials used in the simulation are listed in the table below.

Material	Thermal conductivity at RT, k [W/m K]	Specific heat at RT, C_p [J/kg K]	Density, ρ [kg/m ³]
Silicon	150	710	2330
Aluminum alloy PA6	134	873	2790

Table 1. Physical properties of silicon and aluminum alloy⁴ used in this study.

Geometrical model was subdivided into a 3D network of tetrahedral cells, whose size was adjusted to match the varied length-scales of the heat transport phenomena in this simulation, *i.e.*, with the densest network in the proximity of the illuminated zone and gradually more sparse towards the edges of the system. The smallest cells (cell edge length = 20 μm) were used in the central illuminated region 200 μm \times 200 μm \times 8 mm corresponding to 4 σ_x , 2 z_o and 4 σ_y , respectively.

The simulation took into account only the diffusive mode of heat transfer and assumed no convective heat losses which are minimal in the < 1 Torr vacuum environment of the experiment. Radiative heat losses were also neglected.

5.1. Time dependence

The time necessary to reach the steady-state temperature profile after the laser is turned on can be estimated using an analysis of heat diffusion along the x dimension. This characteristic time, τ_c is related to the characteristic length, $L_c = 6$ mm, assumed to be a half of the Si chip width (symmetric heat flow) and thermal diffusivity of silicon, $\alpha_{Si} = k/\rho \cdot C_p = 88$ mm² s⁻¹ by:

$$\tau_c = \frac{L_c^2}{\alpha_{Si}} \approx 0.4 \text{ s} \quad (3)$$

This characteristic time value is in good agreement with the results of the numerical simulation (Figure S7) what indicates that the steady-state temperature profile under a constant beam power is reached within the first second of illumination.

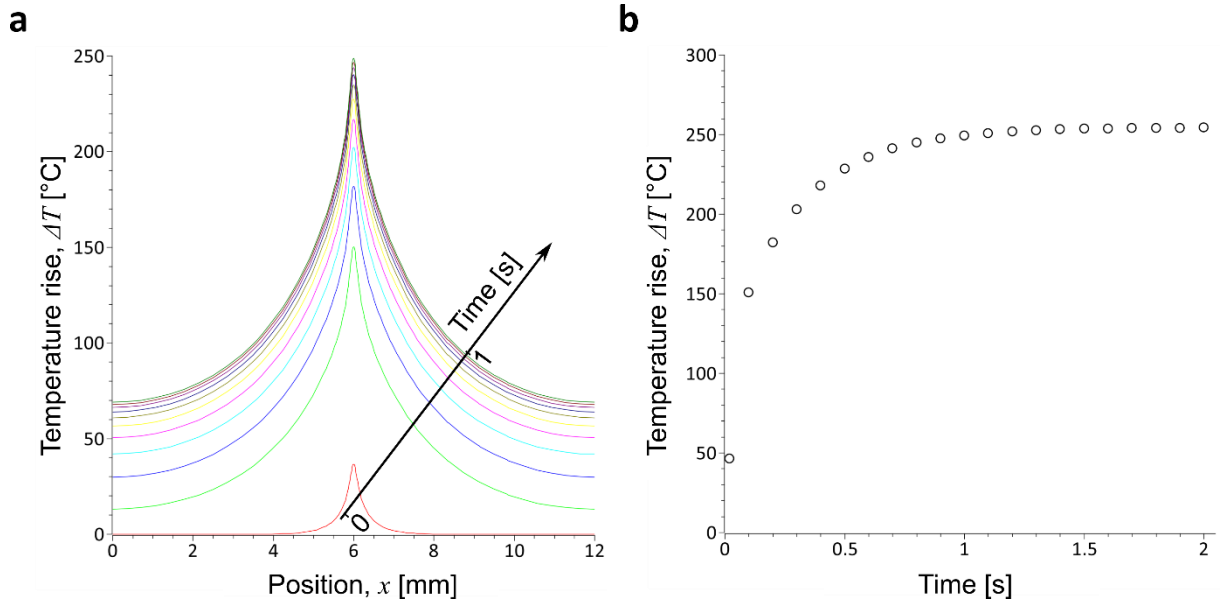


Figure S7. Numerical simulation of time-dependent temperature profile buildup at the surface of Si under illumination with 27 W, 980 nm highly-elongated Gaussian beam ($\sigma_x = 50 \mu\text{m}$ and $\sigma_y = 2.0 \text{ mm}$). a) Temperature profiles across the illuminated zone registered at $t = 0.02$ s (red curve) and from $t = 0.1$ s to 1.0 s in 0.1 s intervals (light green to dark green). b) Time evolution of temperature measured at center of the laser line (peak-temperature location) during the first 2 s of illumination.

Thermal contact between the Si chip and the carrier bar was accounted for as an in-series thermal gap conductance, $h_g \approx 4 \times 10^3 \text{ W m}^{-2} \text{ K}^{-1}$ determined by the gap width, $w_{gap} = 50 \mu\text{m}$ and thermal conductivity of the vacuum grease, k_{eff} filling the gap.

$$h_g = k_{eff} / w_{gap} \quad (4)$$

The estimate of thermal conductivity of the vacuum grease, $k_{eff} \approx 0.22 \text{ W m}^{-1} \text{ K}^{-1}$ is based on the Maxwell-Garnett effective medium approximation:⁵

$$k_{eff} = k_1 \left[\frac{k_2 + 2k_1 - 2\phi_2(k_1 - k_2)}{k_2 + 2k_1 + \phi_2(k_1 - k_2)} \right] \quad (5)$$

Where $k_1 \approx 0.15 \text{ W m}^{-1} \text{ K}^{-1}$ is the conductivity of the PDMS matrix⁶ while $k_2 \approx 1.4 \text{ W m}^{-1} \text{ K}^{-1}$ and $\phi_2 \approx 0.05$ (disclosed information on composition of Dow Corning High Vacuum Grease provided by manufacturer and retailers in the product Safety Data Sheet), are the conductivity and volume fraction of the amorphous silica dispersed phase.^{7,8}

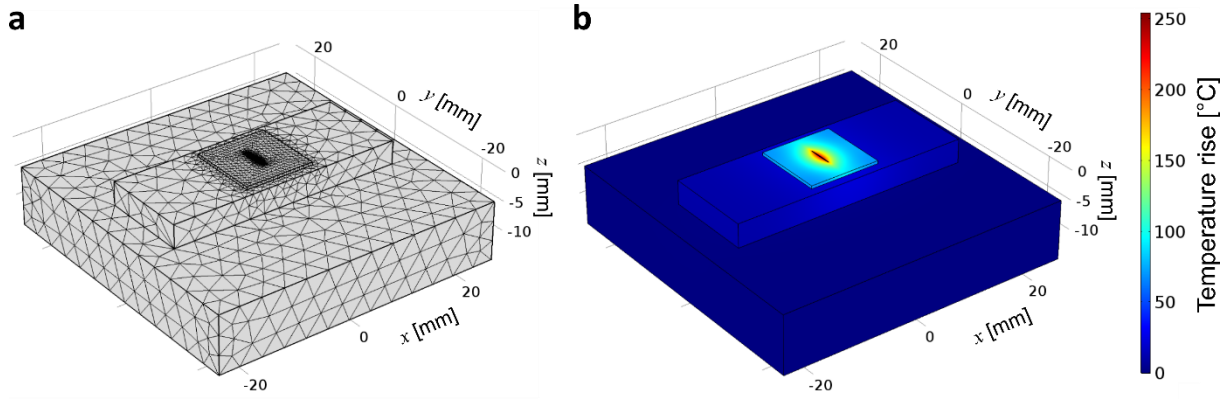


Figure S8. Finite element simulation of heat transport in the laser annealing experiment. a) An overview of the geometry of the 3D simulation model subdivided into tetrahedral simulation cells. b) Temperature rise (ΔT) induced in the Si chip after 30 s of illumination with 27 W, 980 nm highly-elongated Gaussian beam ($\sigma_x = 50 \mu\text{m}$ and $\sigma_y = 2.1 \text{mm}$).

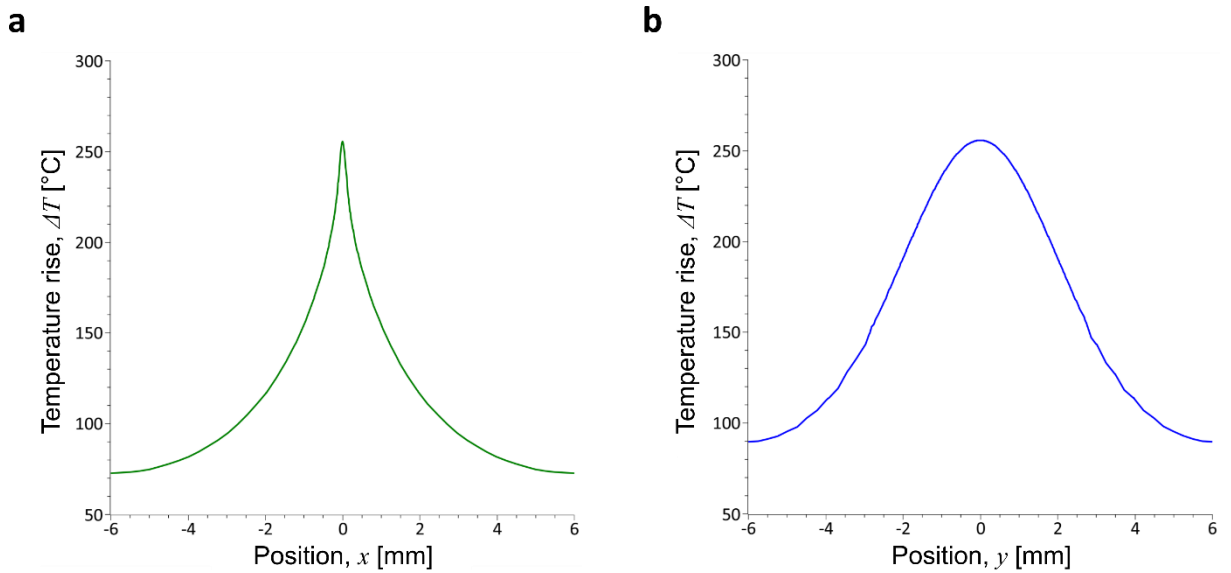


Figure S9. Stationary temperature profiles induced on the Si chip surface after 30 s of illumination with 27 W, 980 nm highly-elongated Gaussian beam ($\sigma_x = 50 \mu\text{m}$ and $\sigma_y = 2.1 \text{mm}$). The rise of temperature across (a) and along (b) the length of the laser line.

Reporting the rise in temperature, rather than the absolute temperature value, is convenient for quick calculation of temperature profiles under different power density of photothermal heat source, *e.g.*, a change in power of illumination or light absorption due to the presence of antireflective coating. For example, lowering the illumination power to 90% of Q_{max} (24 W) and adding a polymer coating, which reduces reflectance coefficient from 31% to 16%, results in the proportional vertical shift of the profile.

$$\Delta T \propto Q$$

$$\Delta T_{polymer,90\%} = 0.90 \times \frac{1 - 0.16}{1 - 0.21} \Delta T_{Si,100\%} \approx 0.96 \Delta T_{Si,100\%} \quad (6)$$

It has to be noted that the resulting temperature field at the surface of the sample is strongly dependent on the value of thermal conductance of the gap. Despite high aerial density of power deposition ($q_{avg} \approx 33 \text{ W mm}^{-2}$ over $fwhm_x \times fwhm_y$ area), the expected rise in temperature of the chip in perfect thermal contact with the supporting bar would only reach 120 °C. Thus, it is critical to reproducibly place the samples on the bar before commencing laser annealing experiments. We designed a convenient gap alignment device or a “*pressing jig*” which guarantees constant and reproducible vacuum grease thickness, $w_{gap} = 50 \mu\text{m}$ used throughout this study (Figure S10).

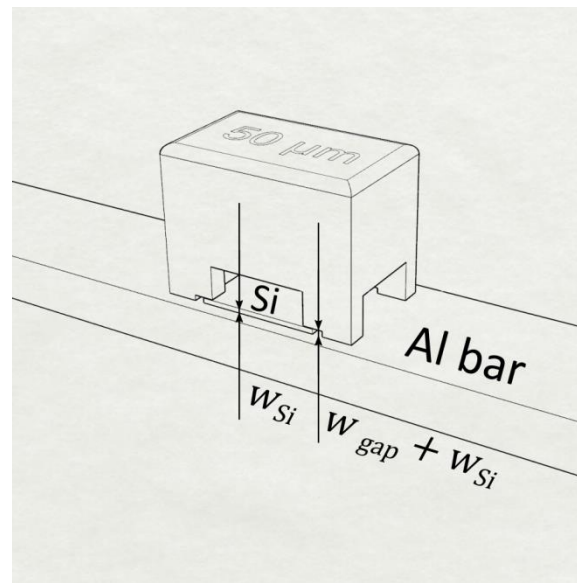


Figure S10. Gap alignment device used to reproducibly mount Si chips on the carrier bar.

5.2. Comparison between laser heating of Si and glass substrates coated with Ge

As previously reported, germanium-coated glass substrates can be used in photothermal annealing experiments utilizing relatively low power laser sources.¹ We have briefly tested such substrates in the current laser annealing setup and observed frequent shattering of the glass slides especially at low rastering velocities (0.1 mm s^{-1}), even at moderate power levels of 5–10 W. The shattering results from accumulation of thermal stresses in glass due to very steep temperature profiles induced in these substrates. Simulated temperature profiles for 1 mm glass slides ($k \approx 1.1 \text{ W m}^{-1} \text{ K}^{-1}$) coated with 100 nm of germanium ($R_{980\text{nm}} \approx 0.4$) are presented in Figure S11. The simulation model assumes complete thermalization of the non-reflected photons in the layer of germanium. At the maximum power level (27 W), the peak temperature would reach $6000 \text{ }^\circ\text{C}$ which exceeds the melting point of glass. It has to be noted that for such substrates the heat transfer is primarily limited by the thermal resistance of the glass layer and only a weak decrease in temperature is observed after the substrates are brought into perfect thermal contact with the carrier bar (Figure S11b).

As discussed in the main text, much lower laser power than in the case of silicon is needed to produce similar thermal fields in the glass substrates of much lower thermal conductivity. To facilitate the comparison between the two substrates, we adjusted the magnitude of incident laser power illuminating the glass/Ge substrates until the simulated temperature profile matched the height of that produced in Si at 27 W (Figure S11c). As expected, such profile is observed at a fraction of laser power required to heat up Si and is also significantly narrower.

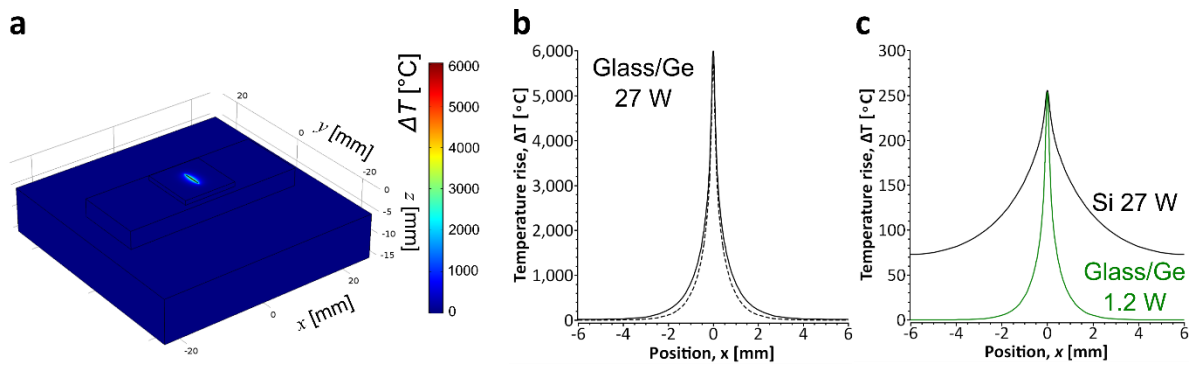


Figure S11. Simulated steady-state surface temperature distribution of the 1 mm thick glass substrates coated with 100 nm Ge under illumination with 27 W, 980 nm highly-elongated Gaussian beam ($\sigma_x = 50 \text{ } \mu\text{m}$ and $\sigma_y = 2.1 \text{ mm}$). a) 3D simulation model. b) Transverse temperature profiles for samples supported by a layer of thermal grease (continuous line) and in perfect thermal contact with the supporting carrier bar (dashed line). c) A comparison between transverse temperature profiles of Si (black line) and glass/Ge substrates (green line) under illumination power intensities matching peak-temperatures of both substrates.

6. Long range alignment

6.1. Sweep velocity influence

It has been previously shown that PS-*b*-P2VP is relatively insensitive to the shear-rate employed in photothermal processing and responds by morphology alignment in SS-LZA experiments performed over a broad range of laser sweep velocities.⁹ In this work however, we have observed that the optimal processing window is somewhat narrower due to an increased risk of thermal damage observed during slow passage of the laser line discussed in Section 7 of SI. The influence of sweep velocity on the degree of morphology alignment at the constant overall time of annealing (≈ 1 min per 1 mm of substrate width) is shown in Figure S12. The order parameter remains constant after the velocity is doubled from 0.32 mm s^{-1} to 0.64 mm s^{-1} and decreases only after it exceeds 1 mm s^{-1} , possibly due to the underheating (convective heat transport due to the motion of the substrate). Conversely, the decrease of sweep velocity below 0.1 mm s^{-1} may lead to better ordering but due to extended residence time in the hot zone, we frequently observed BCP dewetting and PDMS ashing, as shown in Figure S17.

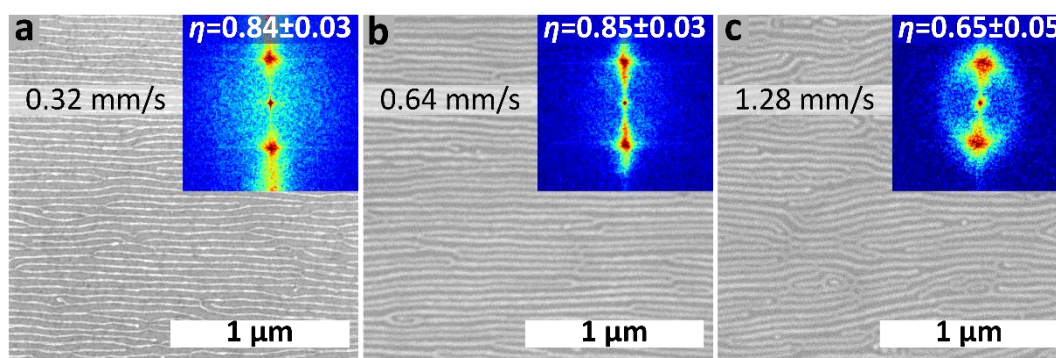


Figure S12. SEM morphologies of C116 PS-*b*-P2VP ordered by soft-shearing at various laser line sweep velocities: a) 0.32 mm s^{-1} , b) 0.64 mm s^{-1} and c) 1.28 mm s^{-1} after 8, 16 and 32 cycles of annealing, respectively. The films were processed using 24 W beam power at $T_b = 90^\circ\text{C}$ and converted to Pt replica after the annealing. The insets present the corresponding FFTs with calculated orientational order parameter values.

6.2. Nanowire arrays and layered meshes

Figure S13 shows a low magnification SEM image of a single layer array of platinum nanowires templated on Si surface from PS-*b*-P2VP C116 aligned after 8 cycles of soft-shearing laser annealing at 0.32 mm s^{-1} using 24 W beam power. The BCP layer can be processed under the same conditions on Si substrates coated with a sacrificial layer of water-soluble poly(styrene sulfonate) sodium salt (PSSS) and then transferred by flotation onto another aligned film forming a BCP bilayer. After metallization the bilayer stack forms a Pt nanomesh (Figure S14).

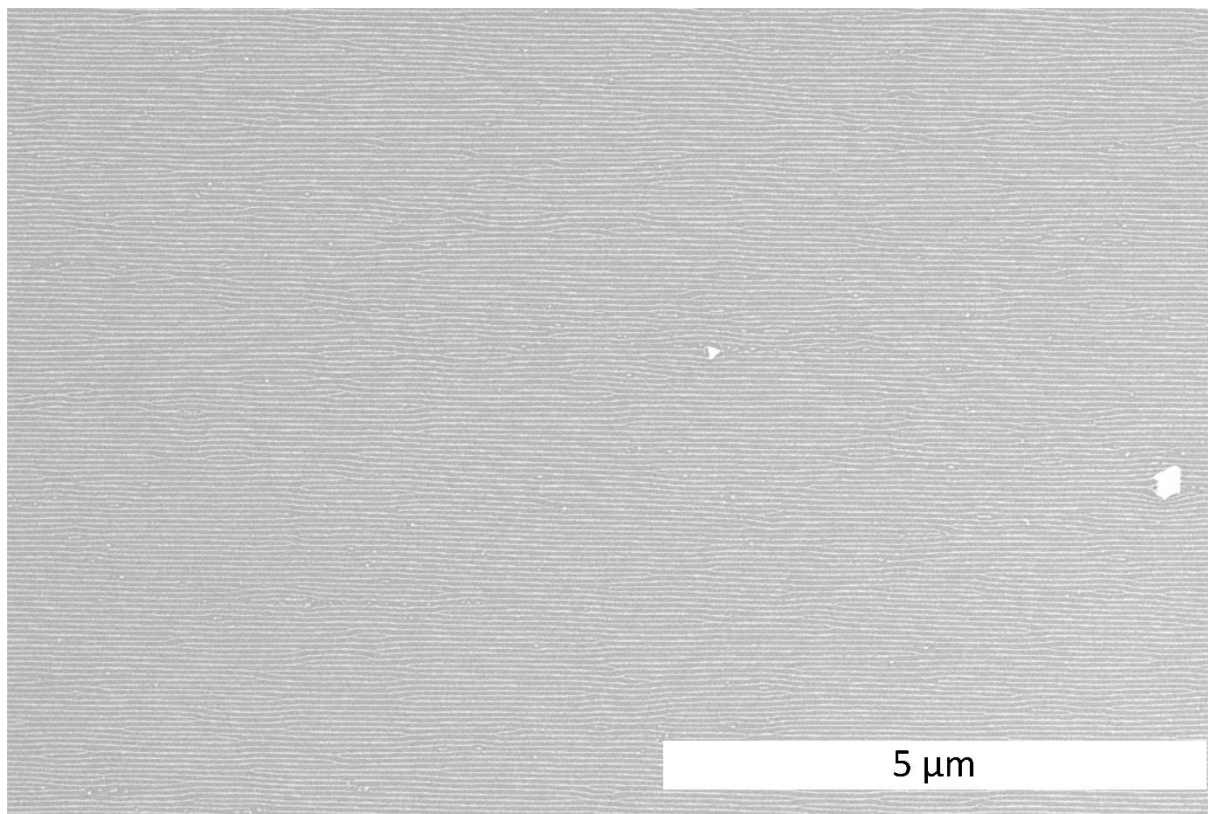


Figure S13. SEM image of Pt nanowires replica C116 S2VP block copolymer after 8 cycles of laser annealing coupled with soft shearing.

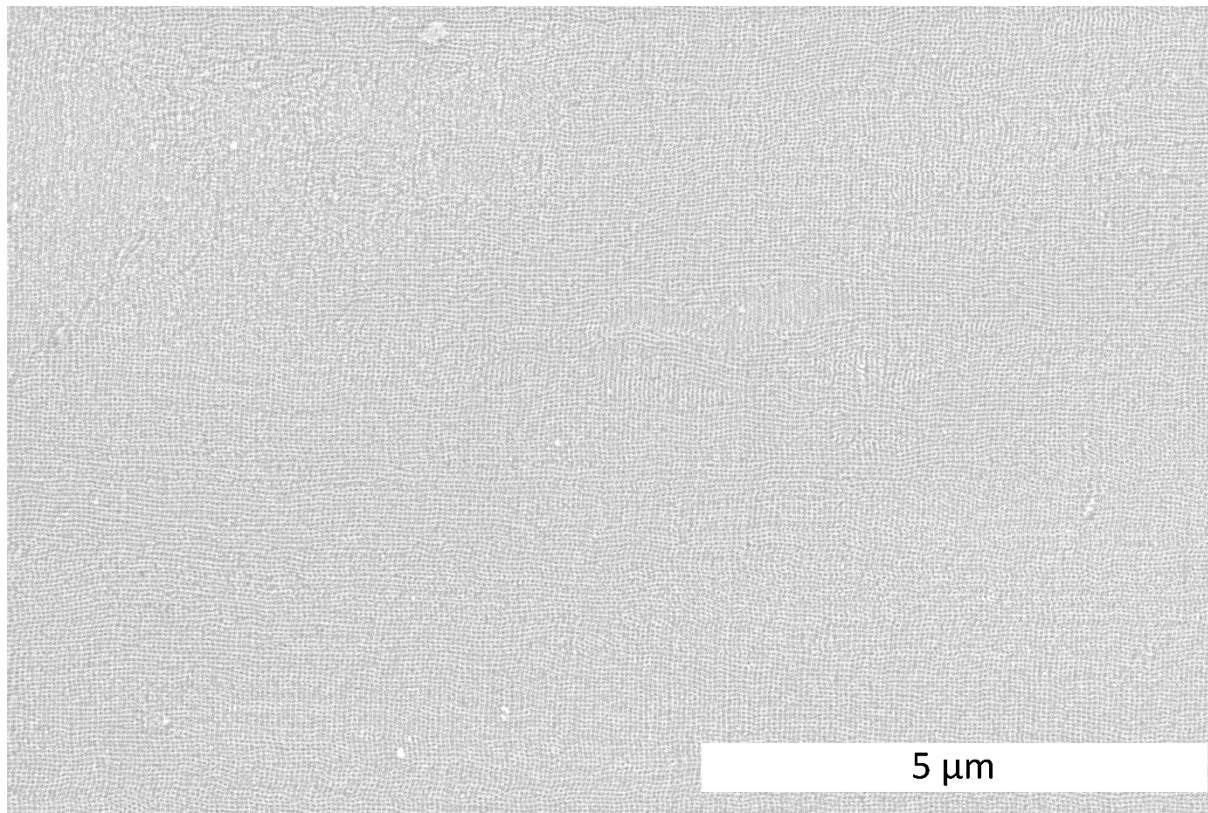


Figure S14. SEM image of Pt nanomesh obtained by wet transfer and vertical stacking of two aligned BCP films. Metallization was performed as the last step after the transfer of the top layer.

Atomic force microscopy (AFM) images acquired in tapping mode reveal the 3D structure of Pt nanowires templated by the laser-aligned PS-*b*-P2VP matrix (C116 S2VP) are shown in figure S15. The average height of the wires is 20 nm.

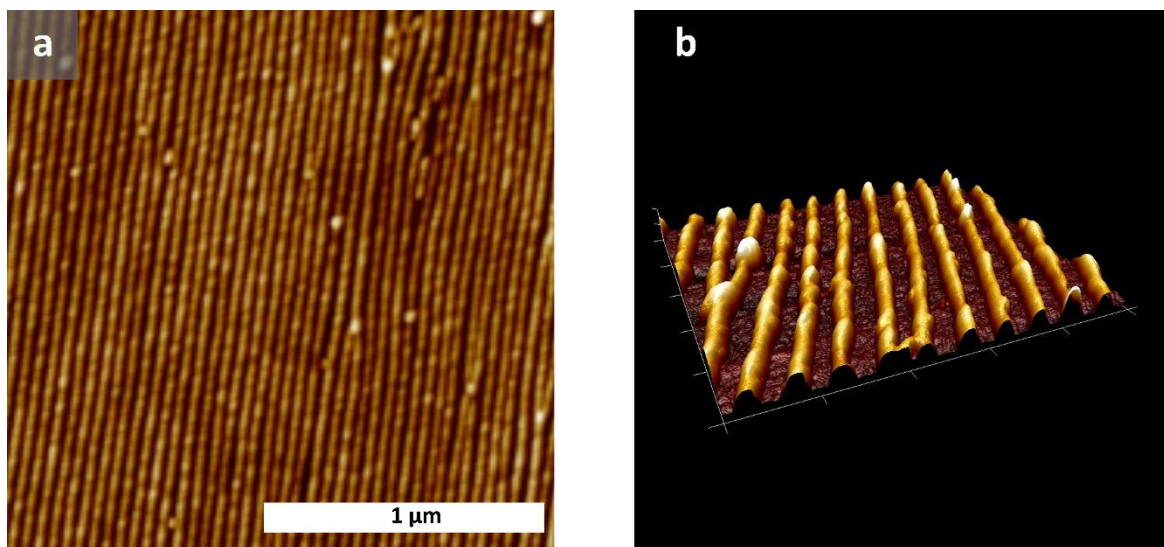


Figure S15. Tapping mode AFM image (a) and a 3D reconstruction (1 μm × 1 μm) (b) of an array of Pt nanowires laser obtained from S2VP C116 BCP after removal of the organic polymer matrix in oxygen plasma.

7. Thermal degradation in laser annealing experiments

Thermal degradation of block copolymers ensues in laser annealing under impermissible experimental conditions, *i.e.*, the combination of high laser power, high base temperature, multiple passages over the same area of film of slowly moving laser line. The last of the listed factors one, together with the width of the thermal zone (w_T), defines the total residence time, t_{res} at and above a particular temperature, T .

$$t_{residence} = n_{passes} \cdot w_T / v \quad (7)$$

In previously reported laser-annealing experiments with a cylinder-forming PS-*b*-PMMA BCPs, thermal degradation was observed if the total residence time, under very slow laser rastering velocity, exceeded $t_{res} \approx 60$ s at temperatures exceeding 300 °C.¹ This result was further corroborated by the findings of Jin *et al.* who more precisely mapped the boundary of thermal-damage for a lamellar PS-*b*-PMMA to 1 s at 350 °C, 10 s at 320 °C, and 100 s at 280 °C.¹⁰ These results are in good agreement with conventional TGA measurements by Lupi and coworkers who reported the onset of thermal degradation for these material to be in the range of 310–320 °C dependent on the molecular weight of the BCP.¹¹ Taking into account their TGA heating rate (20 °C min⁻¹), the residence time at the reported temperatures is approximately 60 s.

Temperature profiles used in this study are notably broader with lower maximum temperatures than those on glass or fused silica substrates due to much higher heat diffusivity of Si substrates. As discussed in the main text, the most effective annealing conditions in terms

of the order parameter of aligned BCP morphologies are produced under reduced laser power and increased base temperature. Figure S16 presents thermal profiles corresponding to the annealing conditions of samples discussed in the main text (Figure 4). The red curve is the optimal profile for soft-shear laser annealing ($P = 24 \text{ W}$, $T_{base} = 90 \text{ }^\circ\text{C}$). At these conditions the residence time at $300 \text{ }^\circ\text{C}$, $t_{300^\circ\text{C}}$ equals 0.7 s during each laser sweep and the cumulative residence time at this temperature is 45 s . Further increase in the laser power, without lowering the T_{base} leads to a rapid increase in the residence time at elevated temperatures. For instance, increasing the laser power by approximately 10% up to 27 W at the same base temperature ($T_{base} = 90 \text{ }^\circ\text{C}$) increases the $t_{300^\circ\text{C}}$ to 1.6 s (cumulatively, 100 s). The increase leads to thermally-damaged BCP morphologies presented in the left panel of Figure S17. Such morphologies in cylindrical PS-*b*-P2VP still exhibit long-range alignment but the minority-block P2VP cylinders are fragmented.

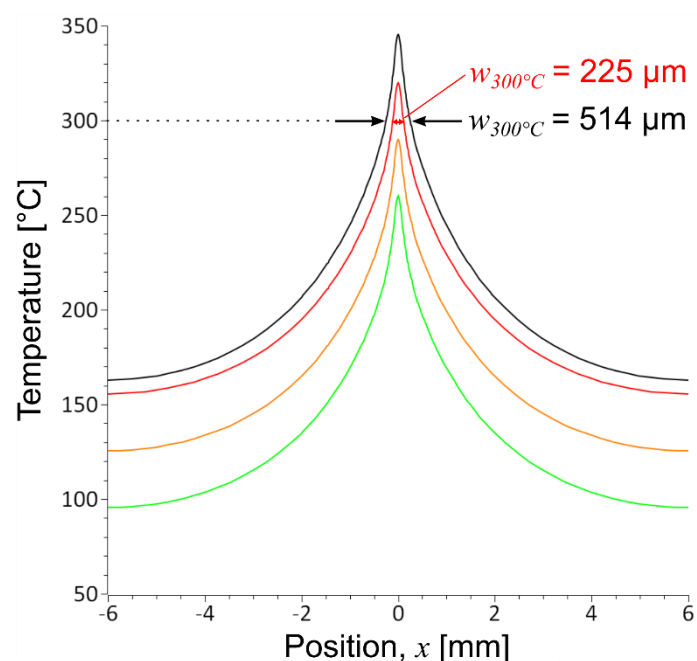


Figure S16. Temperature profiles used in soft-shear laser annealing experiments. Green, orange and red curves represent temperature profiles at $P = 24 \text{ W}$ with $T_b = 30 \text{ }^\circ\text{C}$, $60 \text{ }^\circ\text{C}$ and $90 \text{ }^\circ\text{C}$, respectively. The black curve corresponds to $P = 27 \text{ W}$ and $T_b = 90 \text{ }^\circ\text{C}$.

Severe thermal degradation of polymer film in laser annealing experiments happens when the laser beam illuminates the same spot of the block copolymer film for a prolonged period of time. Figure S17a shows degraded morphology near the scanning direction reversal location where the beam stopped for multiple times after the completion of each annealing cycle and then moved in the opposite direction. Such prolonged stationary beam dwells typically result in the dewetting of the polymer film. Degradation and dewetting can be avoided by turning the laser off during the sweep direction reversal.

Another example of critical beam damage is the uncontrolled thermal run-away in PDMS pad during soft-shear laser annealing experiments, leading to rapid ashing of the elastomer shown in Figure S17b. The milky appearance of the film is caused by the formation SiO_2 particles which are further accelerating the ashing process. According to our observations, this type of thermal degradation happens when PDMS detaches from the BCP film due to a small air cavity

trapped underneath the pad, usually formed by a small imperfection on the surface of the film, e.g. a dust particle. The problem of PDMS ashing can be alleviated by clean laboratory practice minimizing BCP/PDMS interface contamination and by thorough evacuation of air bubbles prior to the annealing experiments.

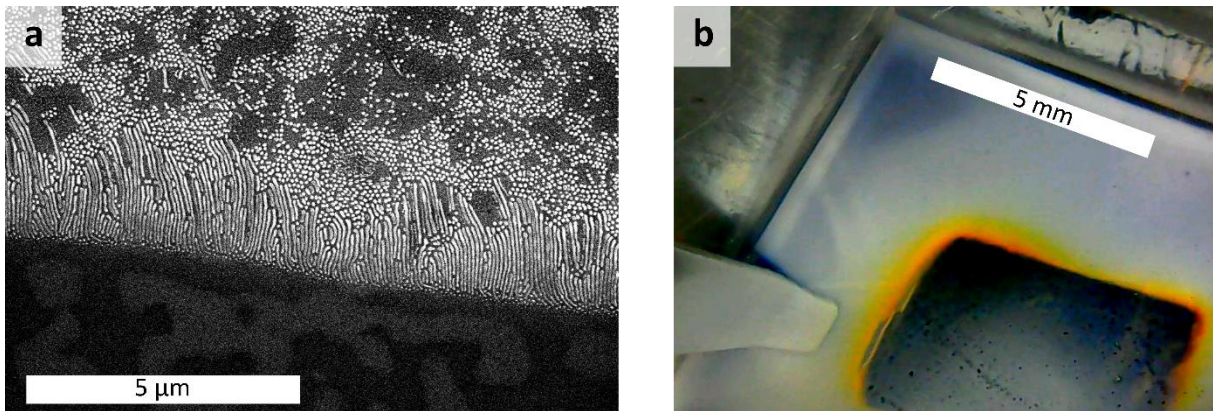


Figure S17. Severe thermal degradation in laser alignment experiments, a) SEM image of the Pt BCP replica near the severe degradation zone with partially dewetted area. b) Macroscopic burn-out of the PDMS pad caused by an uncontrolled detachment of the pad from the BCP surface and subsequent thermal run-away.

8. Oven annealing of cylindrical PS-*b*-P2VP block copolymers

Thermal annealing **in vacuum oven** of cylindrical PS-*b*-P2VP block copolymers with MW \approx 100 kg/mol **in a vacuum oven** yields vertical morphologies in contrast to lower MW homologues which form horizontally-oriented cylinders.

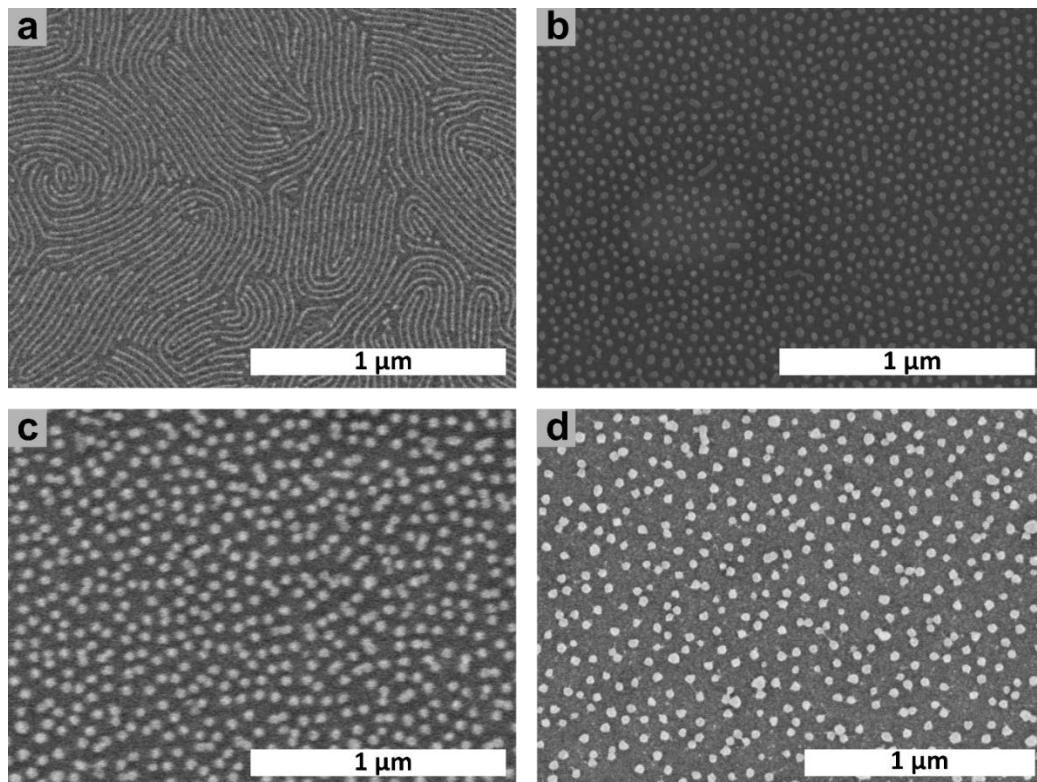


Figure S18. SEM image of C45 (a), C116 (b), C188 (c), C417 (d) PS-*b*-P2VP annealed in a vacuum oven at 200°C for 16 h.

9. References

- (1) Majewski, P. W.; Yager, K. G. Millisecond Ordering of Block Copolymer Films *via* Photothermal Gradients. *ACS Nano* **2015**, *9*, 3896–3906.
- (2) Green, M. A.; Keevers, M. J. Optical Properties of Intrinsic Silicon at 300 K. *Prog. Photovoltaics Res. Appl.* **1995**, *3*, 189–192.
- (3) Jellison, G. E.; Modine, F. A. Optical Absorption of Silicon between 1.6 and 4.7 eV at Elevated Temperatures. *Appl. Phys. Lett.* **1982**, *41*, 180–182.
- (4) ASM Material Data Sheet References
<http://asm.matweb.com/search/SpecificMaterial.asp?bassnum=MA2017T4> (accessed Oct 9, 2019).
- (5) Hong, J.; Choi, H. S.; Lee, K. S.; Shim, S. E. Thermal Properties of Poly(Dimethyl Siloxane) Nanocomposite Filled with Silicon Carbide and Multiwall Carbon Nanotubes. *Polym. Int.* **2012**, *61*, 639–645.
- (6) Lobo, H.; Cohen, C. Measurement of Thermal Conductivity of Polymer Melts by the Line-Source Method. *Polym. Eng. Sci.* **1990**.
- (7) Gao, T.; Jelle, B. P. Thermal Conductivity of Amorphous Silica Nanoparticles. *J. Nanoparticle Res.* **2019**, *21*, 108.
- (8) Dow Corning. Safety Data Sheet Dow Corning High Vacuum Grease
<https://www.2spi.com/item/z05054> (accessed Oct 10, 2019).
- (9) Majewski, P. W.; Yager, K. G. Block Copolymer Response to Photothermal Stress Fields. *Macromolecules* **2015**, *48*, 4591–4598.
- (10) Yong, D.; Jin, H. M.; Kim, S. O.; Kim, J. U. Laser-Directed Self-Assembly of Highly Aligned Lamellar and Cylindrical Block Copolymer Nanostructures: Experiment and Simulation. *Macromolecules* **2018**, *51*, 1418–1426.
- (11) Ferrarese Lupi, F.; Giammaria, T. J.; Seguini, G.; Vita, F.; Francescangeli, O.; Sparnacci, K.; Antonioli, D.; Gianotti, V.; Laus, M.; Perego, M. Fine Tuning of Lithographic Masks through Thin Films of PS-*b*-PMMA with Different Molar Mass by Rapid Thermal Processing. *ACS Appl. Mater. Interfaces* **2014**, *6*, 7180–7188.